Reduction and Simultaneous Removal of ^{99}Tc and Cr by $Fe(OH)_2$(s) Mineral Transformation

Sarah Saslow[1], Wooyong Um[1,*], Carolyn Pearce[1], Mark Engelhard[1], Mark Bowden[1], Wayne Lukens[2], Dong-Sang Kim [1], Michael J. Schweiger [1], and Albert A. Kruger [3]

[1]*Pacific Northwest National Laboratory, 902 Battelle Blvd, Richland, WA, 99352, USA*

[2]*Lawrence Berkeley National Laboratory, 1 Cyclotron Rd, Berkeley, CA, 94720 USA*

[3]*United States Department of Energy, Office of River Protection, P.O. Box 450, Richland, WA 99352, United States*

*Corresponding author: Wooyong Um, Pacific Northwest National Laboratory, 902 Battelle Blvd., PO Box 999, P7-54, Richland, WA 99352, USA. Telephone: (509)-371-7175. Email address: wooyong.um@pnnl.gov

Abstract

Technetium (Tc) remains a priority remediation concern due to persistent challenges, including rapid reoxidation of immobilized Tc, and competing contaminants, e.g. Cr(VI), that inhibit targeted Tc reduction and incorporation into stable mineral phases. Here $Fe(OH)_2$(s) is investigated as a comprehensive solution for overcoming these challenges, by serving as both the reductant (Fe(II)) and immobilization agent to form Tc-incorporated magnetite (Fe_3O_4). Trace metal solution analysis suggests removal of Tc(VII) and Cr(VI) from solution occurs simultaneously; however, complete removal and reduction of Cr(VI) is achieved earlier than Tc(VII). Bulk oxidation state analysis of the solid phase by XANES confirms that the majority of Tc is Tc(IV), which is corroborated by XPS. Furthermore, EXAFS results show successful

Tc(IV) incorporation into magnetite octahedral sites without additional substitution of Cr or Tc into neighboring Fe octahedral sites. XPS analysis of Cr confirms reduction to Cr(III) and the formation of a Cr-incorporated spinel, Cr_2O_3, and $Cr(OH)_3$ phases. Spinel (modeled as Fe_3O_4), goethite, and feroxyhyte are detected in all samples analyzed by XRD, where Tc(IV) incorporation has little effect on the spinel lattice structure. In the presence of Cr(III) a spinel phase along the magnetite-chromite (Fe_3O_4–$FeCr_2O_4$) solid-solution line is formed.

TOC Graphic

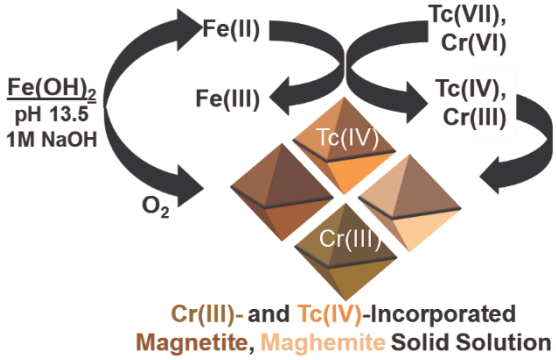

1. Introduction

Nuclear waste generated from processes including fuel recycling and weapon production/testing is a global concern extending beyond well-known legacy sites, e.g. Hanford (Washington State, USA) and Sellafield (Cumbria, UK), creating a universal need for remediation technologies that ensure long-term, safe storage of nuclear waste and contaminant release prevention. One particular concern is 99-technetium (Tc), a radioactive fission product especially problematic due to its long half-life ($2.1x10^5$ years), high fission yield (~6%), and environmental mobility, as Tc(VII) species, in oxidizing subsurface environments.[1,2] Tc remediation from nuclear waste streams has numerous challenges that include: (i) reducing Tc(VII) to less mobile Tc(IV) in the presence of co-mingled contaminants, especially Cr(VI), that are more readily reduced than Tc(VII); and (ii) immobilizing Tc in a form that inhibits reoxidation and subsequent release. Current remediation strategies target these challenges separately, requiring both a reducing agent and immobilizing host material,[3-5] and generates excess cost and residual waste. Herein, $Fe(OH)_2(s)$ is investigated as a silver-bullet approach for simultaneous reduction, removal, and immobilization of Tc and Cr(VI) from waste streams through mineral incorporation.

Iron oxides and hydroxides are common industrial and environmental materials that can facilitate contaminant reduction and incorporate contaminants into their crystal structure, thereby shielding contaminants from re-oxidation. Cr(VI) reduction and immobilization by ferrous materials has been extensively researched for a variety of environmental conditions,[6-8] with reducing agent Fe(II) present in solution[9,10] or as a solid.[11-13] Similar experimental and computational research efforts have investigated Tc(VII),[14-23] with an emphasis on Tc(IV) incorporation into magnetite (Fe_3O_4). Magnetite has an inverse spinel structure,

57 $(Fe^{3+})_{Tet}(Fe^{2+}Fe^{3+})_{Oct}O_4$, where octahedral $Fe(III)_{Oct}$ substitution by metals with similar ionic
58 radii, e.g. Tc(IV), Cr(III), and Ti(IV),[15,24,25] is a common pathway for immobilizing contaminants
59 within the mineral lattice. For example, work performed by Marshall et al.[15] reports successful
60 incorporation of reduced Tc(IV) into the magnetite structure under the high pH conditions
61 expected to persist in nuclear waste streams.

62 Heretofore the simultaneous reduction, removal, and incorporation of co-mingled Tc(VII)
63 and Cr(VI) has not been studied. Building upon success immobilizing Tc(IV) in magnetite, the
64 approach described here forms magnetite via mineral transformation of $Fe(OH)_2(s)$ under oxic
65 conditions via the Schikorr reaction.[26,27] $Fe(OH)_2(s)$ in solution concurrently reduces Tc(VII) and
66 Cr(VI) to Tc(IV) and Cr(III) and incorporates both contaminants into the magnetite structure. In
67 addition, the mechanism by which Tc(VII) and Cr(IV) are reduced and immobilized are
68 investigated using a suite of analytical tools to probe the oxidation state, local coordination
69 environment, and properties of the solid phases formed at the molecular-level.

70 **2. Experimental**

71 **$Fe(OH)_2(s)$ Synthesis.** $Fe(OH)_2(s)$ was prepared inside an anoxic chamber (Coy laboratories)
72 maintained with a gas mix of N_2 (98%) and H_2 (2%), an H_2/O_2 gas analyzer, and a palladium
73 catalyst for O_2 removal. $Fe(OH)_2(s)$ was precipitated by dissolving 14 g of $FeCl_2 \cdot 4H_2O$ (>95%,
74 Fisher Scientific) in 400 g of double deionized water (DDI, Millipore 18Ω) pre-purged with N_2,
75 adding 8.2 mL of 10M NaOH (prepared from 95% NaOH pellets, Fisher Scientific), and then
76 mixing. After reacting overnight, $Fe(OH)_2(s)$ was filtered using a sterile 0.45 μm analytical filter
77 (Nalgene) and allowed to dry for 24-48 hours. Prior to experimentation, oxidized surface
78 material (if present) was removed to expose un-oxidized $Fe(OH)_2(s)$ that was then reduced to a
79 powder by mortar and pestle and appropriately measured no more than 24 hours before use.

Solution Preparation. In this work a background solution of 1M NaOH (prepared from 95% NaOH pellets, Fisher Scientific), was adjusted to 1560 ppm Cr(VI) with $Na_2Cr_2O_7 \cdot 2H_2O$ (≥99.5%, Allied Chemical) to achieve an alkaline pH level and Cr(VI) concentration similar to nuclear waste streams.[28] For experiments requiring Tc(VII), a 10,000 ppm NH_4TcO_4 stock solution was used to adjust Cr(VI) solutions to within 1 and 1000 ppm Tc(VII). For control experiments, without Cr(VI), Tc(VII) was added directly to 1M NaOH.

Procedure for Tc(VII) and Cr(VI) Reduction and Removal by $Fe(OH)_2(s)$. Tc(VII) and Cr(VI) reduction and incorporation into iron oxides was assessed using the following procedure. Approximately 0.01 to 0.5 g of $Fe(OH)_2(s)$ was added to solution immediately after removal from the anoxic chamber. Once combined the samples were reacted for 3 days (±1 hour) in an oven set to 75°C, after which the oven was turned off and the samples allowed to cool inside the oven for at least two hours. The solid material was then filtered (0.45 μm sterile analytical filter, Nalgene), rinsed with ~50 mL of DDI, and air-dried for at least 24 hours. While filtering, samples of the supernatant and DDI rinse were collected for total Cr analysis by Inductively Coupled Plasma-Optical Emission Spectrometry (ICP-OES) and total Tc analysis by ICP-Mass Spectrometry (ICP-MS). The final measured pH of a representative sub-set of samples was 13.5 ± 0.1.

For select samples, the above procedure was altered to test whether sequential addition of $Fe(OH)_2(s)$ impacted the reduction and immobilization process of Tc(VII) and Cr(VI). For these samples, $Fe(OH)_2(s)$ was sequentially added over three days, allowing the solution to react with the solid for ~24 hours before adding additional $Fe(OH)_2(s)$ or final sampling. An aliquot was taken for ICP-OES and ICP-MS analysis before each subsequent addition to monitor Tc(VII) and Cr(VI) removal. Additional procedure details and test matrix are provided in the supporting

information (SI, Section S1 and Table S1).

Cr Speciation by Ion Chromatography (IC)/ICP-MS. The details of this procedure may be found in the SI. Briefly, select samples analyzed for Cr(VI) and Cr(III) in the collected supernatant were separated using a chrom-FAST Chromium 3/6 Speciation Kit (CF-KIT-Cr36) and SC-DX FAST auto sampler (Elemental Scientific Corporation (ESI)). ^{52}Cr was the primary mass analyzed while ^{53}Cr was monitored for confirmation purposes. Cr(III) and Cr(VI) were analyzed quantitatively using a Perkin Elmer ELAN DRC II quadrupole ICP-MS using time resolved data points. Chromatographic peak areas were integrated using periSPEC Peak Area Finder software (ESI).

X-ray Photoelectron Spectroscopy (XPS). XPS was used to evaluate the chemical composition and oxidation state of Cr, Fe, and Tc at the sample near surface as a function of $Fe(OH)_2$(s):solution ratio and starting Tc(VII) concentration. For Tc-free samples, XPS measurements were performed using a Physical Electronics Quantera Scanning X-ray Microprobe equipped with a focused monochromatic Al Kα X-ray (1486.7 eV) source for excitation and a spherical section analyzer. The 80 W X-ray beam was focused to 100 μm diameter and rastered over the sample. High energy resolution spectra were collected using a pass-energy of 69.0 eV and 0.125 eV step size. Tc-containing samples were analyzed using a Kratos Axis DLD spectrometer with a monochromatic Al Kα X-ray (1486.7 eV) source. Spectra were charge-corrected to the main line, carbon 1s peak (adventitious carbon) at 285.0 eV. Data analysis and peak fitting was performed in CasaXPS (version 2.3.15). XPS peak fitting procedures are detailed in the SI.

X-ray Diffraction (XRD). XRD spectra were collected using a Rigaku Miniflex II XRD unit equipped with a Cu Kα radiation (λ=1.5418 Å with 30 kV and 15 mA) source. Samples

containing an internal standard, ~10 wt% corundum (NIST standard) or rutile (NIST or Sigma Aldrich, CAS # 224227), were scanned at minimum between 3 and 90 degrees 2θ in fixed mode using a 0.05 degree step size and 20 seconds/step scan speed. Mineral identification was completed using Jade software (Materials Data Incorporated, California) with reference spectra from the International Centre for Diffraction Data XRD database. Rietveld quantification refinements were performed using Bruker TOPAS software (v5, Bruker AXS, Germany) with reference patterns from published crystal structures (Inorganic Crystal Structure Database, Fachinformationszentrum Karlsruhe, Germany). Mineral phase fractionation was scaled to 100% by reference to the internal standard. Additional procedure details are provided in the SI.

Scanning Electron Microscopy (SEM) and Energy Dispersive Spectrometry (EDS). Before SEM/EDS analysis, select samples were homogenized in a mortar and pestle, mounted on an aluminum stub with double-sided carbon tape, and sputter coated with Pt (Polaron Range SC7640, Quorum Technologies Ltd., East Sussex, England). SEM analysis was performed using a JSM-7001F field-emission gun microscope (JEOL USA, Inc., Peabody, MA); EDS was performed using a Bruker xFlash 6|60 (Bruker AXS, Inc., Madison, WI). The acceleration voltage during imaging was 15 kV. For all analyses, Kα positions were considered for the calculations. The EDS spectra were collected for 20 s each at 80 k–100 k counts/s. Background noise subtraction and atomic ratio estimates were performed using ESPRIT software (v1.9, Bruker AXS, Inc.).

X-ray Absorption Near Edge Structure (XANES) and Extended X-ray Absorption Fine Structure (EXAFS) Spectroscopy. XANES and EXAFS were used to determine the bulk oxidation state and local coordination environment, respectively, of Tc once reduced and immobilized within the magnetite crystal structure. Analysis was limited to samples with starting

Tc concentrations ≥11 ppm (XANES) and ≥100 ppm (EXAFS). Tc K edge (21044 eV) spectra were collected on beamline 11-2 at the Stanford Synchrotron Radiation Laboratory (SSRL). Dead-time correction and data reduction was performed using SixPack.[29] Data analysis was performed using ATHENA/ARTEMIS software.[30] XANES spectra were energy calibrated using TcO_4^- adsorbed on Reillex-HPQ and fit using a linear combination of Tc(IV) and Tc(VII) standards.[31] For EXAFS fitting, a Tc-substituted magnetite structure was used in addition to models for $TcO_2 \cdot 2H_2O$ and TcO_4^- as necessary.[14,31,32] Additional analysis details are provided in the SI.

3. Results and Discussion

Tc(VII) and Cr(VI) Removal by $Fe(OH)_2$(s). Percent removal of Cr and/or Tc from solution was determined as a function of $Fe(OH)_2$(s):solution ratio (Figure 1). In the absence of Cr(VI), 1 ppm of Tc(VII) is removed (>99.5%) with a minimum $Fe(OH)_2$(s):solution ratio of 0.005 g/mL; however, in the presence of 1560 ppm Cr(VI), an $Fe(OH)_2$(s):solution ratio of 0.02 g/mL is required to completely remove Cr(VI) and Tc(VII) (>99.7%). This same $Fe(OH)_2$(s):solution ratio is required to remove Cr(VI) from solution in the absence of Tc(VII).

Assuming Cr(VI) and Tc(VII) removal is contingent on reduction to Cr(III) and Tc(IV) first, the Fe(II) required for reduction can be assessed as follows. Cr(VI) and Tc(VII) require three electrons each for reduction to Cr(III) and Tc(IV).[33]

$$\mathrm{Cr(VI)O_4^{2-} + 5H^+ + 3e^- = Cr(III)(OH)_{3(s)} + H_2O} \quad \mathrm{E^\circ = 1.34V} \qquad \text{(Eq. 1)}$$

$$\mathrm{Tc(VII)O_4^- + 4H^+ + 3e^- = Tc(IV)O_2 \cdot \mathit{n}H_2O_{(s)} + (2-\mathit{n})H_2O} \quad \mathrm{E^\circ = 0.75V} \qquad \text{(Eq. 2)}$$

Provided that Cr(VI) and Tc(VII) are present in solution at a combined concentration of 0.030 eq/L, only 0.09 Fe(II) eq/L is required for complete reduction to Cr(III) and Tc(IV). The experimentally determined $Fe(OH)_2$(s):solution ratio needed to remove Tc(VII) and Cr(VI) from

solution, 0.02 g/mL, is equivalent to 0.22 Fe(II) eq/L and over double the required Fe(II) equivalents needed. Excess Fe(II) is likely needed to off-set rapid oxidation of Fe(II) to Fe(III) under oxic conditions and generate Fe(III) necessary to form iron oxide phases, such as magnetite ($Fe^{2+}Fe_2^{3+}O_4$) and goethite (α-FeOOH), capable of incorporating Cr(III) and Tc(IV) into their mineral structure.[12,13,15,20,21]

Surprisingly, when Cr(VI) and Tc(VII) are both present in solution, reduction and removal of both constituents occurs concurrently, despite a more favorable reduction potential for Cr(VI) versus Tc(VII), 1.34 V and 0.748 V, respectively.[33] This is most evident in Figure 1, where if Cr(VI) was completely removed before Tc(VII), an increase in Tc(VII) removal would not be observed with partial removal of Cr(VI) at $Fe(OH)_2$(s):solution ratios between $2.5x10^{-3}$ and 0.01 g/mL.

Cr(VI) Reduction by $Fe(OH)_2$(s).

Speciation of Cr Remaining in the Supernatant. From preliminary control experiments focusing on the removal of Cr(VI) in the absence of Tc(VII), two duplicate samples were analyzed by IC/ICP-MS to determine the speciation of Cr remaining in solution, after partial removal by $Fe(OH)_2$(s) ($Fe(OH)_2$(s):solution ratio, 0.01 g/mL). For both samples, Cr was 85(1)% removed from solution. Samples were analyzed for Cr(VI) and Cr(III) using isotopes ^{52}Cr and ^{53}Cr. Table 1 reports these values and the isotopic average. The non-detect levels of Cr(III) by this method confirm that Cr remaining in the supernatant is almost completely Cr(VI).

Speciation of Cr in the Solid Phase. The speciation of Cr was analyzed by XPS for select solid samples. XPS high resolution narrow scans for Cr are shown in Figure 2A for three Cr-containing solid samples (no Tc) for $Fe(OH)_2$(s):solution ratios 0.005, 0.01, and 0.06 g/mL. Peak fitting was performed only for the Cr $2p_{3/2}$ peak, due to the complexity of the Cr region. Cr(VI)

193 was fit as one peak and Cr(III) species fit separately as Cr_2O_3, chromite ($FeCr_2O_4$), and $Cr(OH)_3$.
194 Procedure details for peak fitting are provided in SI, section S2, and a phase distribution
195 summary is provided in Table 2. From peak fitting results, <6.91 atomic (at) % Cr(VI) is present
196 on the sample near surface (top ~10 nm), with the remainder of the Cr present as Cr(III)
197 incorporated into the spinel phase (modeled as chromite, $FeCr_2O_4$) or as Cr_2O_3 and $Cr(OH)_3$.
198 The distribution of Cr(III) between the three modeled phases can be justified when
199 considering the Cr:Fe ratio detected on the surface (Table 2), determined from the relative XPS
200 surface composition (Table S3). At a 0.005 g/mL $Fe(OH)_2$(s):solution ratio, the sample near
201 surface has a Cr:Fe ratio of 4.39 and only 9.24 at% Cr is incorporated as $FeCr_2O_4$. The remaining
202 Cr(III) is mostly distributed between Cr_2O_3 and $Cr(OH)_3$. However, an increase in the
203 $Fe(OH)_2$(s):solution ration, to 0.01 g/mL, lowers the surface Cr:Fe ratio to 1.52 and increases
204 Cr(III) incorporation into chromite to 47.3 at%. This chromite increase is consistent with similar
205 work[9] and attributed to an increase in Fe(II) available to reduce Cr(VI) and incorporate Cr(III)-
206 into $FeCr_2O_4$. Deviation from this trend is observed at an $Fe(OH)_2$(s):solution ratio of 0.06 g/mL,
207 where nearly 97 at% Cr is associated with Cr_2O_3 and $Cr(OH)_3$; however, given the extremely low
208 Cr:Fe ratio, 0.12, little Cr is present on the surface. This is likely due to the presence of excess
209 Fe(II) that forms an Fe-oxide passivation layer on the surface of Cr-containing solids. The
210 presence of a passivation layer is supported by the spinel parameter calculated from respective
211 XRD spectra, where there is an increase in magnetite-like structure with decreasing Cr:Fe ratio
212 (Table 2).
213 SEM images and EDS measurements provided in the SI (Section S4) further support an
214 increase in spinel and Cr-incorporated spinel phase formation with a decrease in the starting
215 concentration ratio of Cr:Fe. This is evident from the near micron size spinel crystals imaged at

lower Cr:Fe ratios and the composition determined by EDS matches that of magnetite within error (43 at% Fe and 57 at% O).

Tc(VII) Reduction by $Fe(OH)_2$(s). A mechanism similar to that for Cr(VI) reduction and incorporation is expected for Tc(VII). The oxidation state of Tc in the solid phase was determined by XANES. XANES spectra were fit (Figure 3, left panel) using a linear combination of TcO_4^- and $TcO_2 \cdot 2H_2O$ standards to determine the fraction of Tc(VII) and Tc(IV) species (Table 3). As expected, an increase in the initial Fe:Tc ratio, calculated from the moles of Tc and Fe(II) added at the start of the experiment (SI Section S5), correlates with an increase in reduction of Tc(VII) to Tc(IV); however, some Tc(VII) is still present at the lowest Fe:Tc molar ratio. This could be due to Tc(IV) reoxidation to Tc(VII), TcO_4^-, between sample preparation and analysis (~3 weeks). For all other samples analyzed by XANES, little to no Tc(VII) is present. Furthermore, based on these results, Cr does not seem to hinder the reduction of Tc(VII) despite redox potentials ((Eq. 1 and (Eq. 2) favoring Cr reduction.

For comparison, samples analyzed by XANES were also analyzed by XPS to compare bulk phase results to those of the near surface. A summary of these results is provided in Table 3 and detailed in SI, Section S2. Overall the presence of Tc on the sample near surface is minimal, ranging from 0 to 0.81 at% with decreasing Fe:Tc ratio. Tc $3d_{5/2}$ and $3d_{3/2}$ peak fitting of high resolution narrow scans (Figure 2B) show an increase in Tc(IV) on the sample surface with increasing Fe:Tc, ranging from 57.64% to 84.35% for those samples where Tc was detected. Since XPS is surface sensitive and XANES characterizes the bulk phase, XPS detection of Tc(VII) on the surface of samples otherwise undetectable by XANES is not surprising, though does not discount the efficacy of $Fe(OH)_2$(s) for the reduction and removal of Tc(VII) based on

238 the trends described. Some re-oxidatiokn of Tc(IV) is expected upon exposure to air over
239 extended time periods,[15] a challenge that will be targeted in future work.

240 **Local Coordination Environment of Tc(VII) by EXAFS.** $Fe(OH)_2$(s) suspended in
241 solution will rapidly form magnetite (Fe_3O_4) under oxidizing conditions. The formation of
242 magnetite is driven by electron transfer between Fe(II) and Fe(III) ions and dissolution
243 crystallization, depending on available Fe(II) and metal ion substitution into the crystal
244 structure.[34] During this transformation, Tc(IV) can easily be incorporated into the mineral
245 structure, as it has the same ionic radii as Fe(III), 0.785Å,[35] thereby protecting Tc(IV) from
246 reoxidation. To evaluate Tc(IV) incorporation into magnetite in the presence of Cr(VI)/Cr(III)
247 the local coordination environment was determined for select samples by EXAFS. Figure 3
248 (middle and right panels) shows collected EXAFS spectra, their Fourier transforms, and fits. A
249 Tc-incorporated modified magnetite model[32] was used to fit all samples, with some samples
250 requiring additional pathways to account for Tc(IV) precipitated on the surface, modeled by
251 $TcO_2 \cdot 2H_2O$,[31] and surface pertechnetate (TcO_4^-).[14] EXAFS fit parameters for samples and
252 models are outlined in Tables S7 and S8, respectively. A Tc-incorporated goethite (α-FeOOH)
253 model was also considered during early stages of analysis, but failed to accurately fit the data.
254 Partial substitution of Tc and/or Cr into the nearest neighboring Fe octahedral site (Fe1, S7) did
255 not improve any sample fits. Finally, including first shell oxygen at 2.47Å to account for
256 hydrated oxygen in $TcO_2 \cdot 2H_2O$ did not contribute significantly to the sample fit for Fe:Tc ratio
257 491, despite the presence of Tc at ~2.57Å. This is attributed to $TcO_2 \cdot 2H_2O$ Tc(IV) atoms being
258 partially incorporated into magnetite, convoluting signal due to TcO_2 hydration.[15,36,37]

259 Based on the coordination numbers determined from EXAFS fits, the fractional composition
260 of each sample was determined for TcO_4^-, $TcO_2 \cdot 2H_2O$, and Tc-incorporated magnetite (Table 3)

and is graphically shown in Figure 4. The results agree with the fraction of Tc(VII) versus Tc(IV) determined by XANES. From Figure 4, it is apparent that with increasing Fe:Tc there is a steady increase in Tc-incorporated magnetite; however, total incorporation of Tc into magnetite is not achieved at the Fe:Tc ratios analyzed. For a 56 Fe:Tc ratio, with no Cr added, Tc is largely present as $TcO_2 \cdot 2H_2O$ and TcO_4^-, with only 17(5)% Tc incorporated into magnetite. The high p value (0.082) associated with incorporating octahedral Fe (magnetite, Fe1) indicates that it does not significantly improve the fit and supports Tc mostly present as $TcO_2 \cdot 2H_2O$ and TcO_4^-. Alternatively, when 1560 ppm Cr is added, Tc-incorporated magnetite increases to 20(4)% and TcO_4^- decreases from 28(2)% to 10(2)%. This suggests Tc(VII) reduction is not hindered by Cr(VI) and the formation of Cr-oxide/hydroxide passivation layers (XPS Analysis, Table S2) could reduce risk of Tc(IV) reoxidation and dissociation from magnetite.[12,13] For larger Fe:Tc ratios, 208 and 491, TcO_4^- is not detected, and while $TcO_2 \cdot 2H_2O$ remains the dominant Tc phase, Tc-incorporated magnetite steadily increases with Fe:Tc ratio, reaching a maximum of 44(5)%. This trend is consistent with previous for larger Fe:Tc ratios, where Tc-incorporated magnetite is the dominant Tc phase.[21,23]

Solid Phase Characterization by XRD. Solid mineral phase distribution as a function of $Fe(OH)_2$(s):solution ratio, Cr(VI) and Tc(VII) concentration was determined by XRD. Previously mentioned, a decrease in the magnetite lattice a parameter, 8.396 Å, to values near 8.378 Å (chromite) or 8.34 Å (maghemite, γ-Fe_2O_3) can elucidate ion substitution and mineral transformation processes.[38,39] Figure 5 provides examples of XRD patterns for samples exposed to Cr(VI) and/or Tc(VII), a control sample (no Cr(VI) or Tc(VII)), and reference spectra for magnetite, feroxyhyte (δ-FeO(OH)), and goethite. From quantification and refinement calculations (Table S4), the primary phases present in all samples are goethite, feroxyhyte,

spinel, and amorphous (unidentified) phases. Since magnetite, chromite, and maghemite spinels could not be individually resolved, quantification and refinement calculations only incorporate one spinel phase, magnetite.

At low concentrations, 1 ppm, Tc is expected to be predominantly incorporated into the magnetite structure based on the increase in Tc incorporation extrapolated from EXAFS phase distributions (Figure S8). This assumption is supported by the calculated spinel a parameter, 8.3944(2) Å, which nearly matches magnetite (8.396 Å)[38,39] and indicates negligible distortion of the crystal structure upon Tc incorporation. Additionally, compared to the control sample formed in the absence of Tc and Cr(VI), spinel formation increased from 27% to 48%, suggesting that the presence of Tc might drive spinel formation over other phases.

Detailed previously, Cr(VI) addition drives the spinel a parameter closer to that of chromite. When 1 ppm Tc is co-mingled with Cr(VI), the spinel phase formed is minimally effected by the presence of Tc and maintains a chromite-like a parameter, 8.3785(6) Å. However, at elevated Tc concentrations, ~100 ppm, a slight increase in the a parameter is observed (~8.386 Å), suggesting that Tc-incorporation into the spinel phase is more favorable than Cr(III) incorporation. This could be due to the match in ionic radius between Tc(IV) and Fe(III), where the slightly smaller ionic radius for Cr(III), 0.755 Å,[40] is less favorable for incorporation. However, chromite adapts a normal spinel structure, where Fe(II) occupies the tetrahedral sites and Cr(III) occupies the octahedral sites. Tc can easily be incorporated into the magnetite structure without disturbing the inverse spinel crystal structure, as the data supports. However, formation of chromite would require topotactic rearrangement of initially-formed magnetite to incorporate Cr(III) and continue chromite formation. The energy barrier to undergo this

306 rearrangement from an inverse to normal spinel structure is proposed here to be less favorable
307 than the incorporation of Tc(IV) into magnetite.

308 Further investigation into this hypothesis is required, specifically to verify that magnetite and
309 chromite are the only two phases contributing to the spinel fraction, since the presence of
310 maghemite would also decrease the spinel lattice parameter, a.[35,41] A comparison of samples
311 prepared under identical conditions, but analyzed by XRD within 30 days of sample preparation
312 or 30 days (or more) after preparation, show a decrease in the spinel a parameter with aging. This
313 is not surprising given that in air magnetite undergoes maghematization, in which Fe(II) is
314 oxidized to Fe(III) and the migration of excess Fe(III) atoms to the surface produces a film of
315 maghemite (γ-Fe_2O_3).[42] The effect of maghematization will be the focus of future studies.

316 **Environmental Implications.** Successful reduction and immobilization of Tc(VII) and
317 Cr(VI) by $Fe(OH)_2$(s) mineral transformation provides a viable approach to treating nuclear
318 waste streams containing co-mingled Tc(VII) and Cr(VI), serving as both a reductant and
319 immobilizing agent. Once incorporated into the magnetite structure Tc(IV) is less susceptible to
320 reoxidation induced by changes in the surrounding environment, providing valuable remediation
321 opportunities for waste processing and in the natural environment. For example, Tc-incorporated
322 magnetite could be introduced into the proposed vitrification waste stream at the DOE Hanford
323 site, where magnetite-stabilized Tc would be less likely to volatilize under vitrification
324 temperatures, thus increasing Tc loading in glass waste forms. While the stability of Tc-
325 incorporated magnetite under vitrification temperature conditions is the focus of ongoing work,
326 successful integration of this work, using $Fe(OH)_2$(s), can also be applied to remove both Tc and
327 Cr from secondary off-gas scrubber waste streams for reducing the risk of remobilization into the
328 environment.

4. Acknowledgements

This research was supported by the U.S. Department of Energy's (DOE) Waste Treatment and Immobilization Plant Project of the Office of River Protection. PNNL is operated for the DOE by Battelle Memorial Institute under Contract DE-AC05-76RL0 1830. The XANES and EXAFS data collection was carried out at the SSRL, a national user facility operated by Standard University on behalf of the US DOE. A portion of the solid characterization was performed using EMSL and RadEMSL, a national scientific user facility sponsored by the Department of Energy's Office of Biological and Environmental Research and located at Pacific Northwest National Laboratory. A portion of this work (WWL) was supported by the U.S. Department of Energy, Office of Science, Basic Energy Sciences, Chemical Sciences, Biosciences, and Geosciences Division (CSGB), Heavy Element Chemistry Program and was performed at Lawrence Berkeley National Laboratory under contract No. DE-AC02-05CH11231

5. Supporting Information

Additional analysis procedures and results for $Fe(OH)_2(s)$ addition, IC/ICP-MS, XPS, XRD, SEM/EDS, XANES, and EXAFS are provided in the supporting information via the Internet at http://pubs.acs.org.

6. References

(1) Darab, J. G.; Smith, P. A. *Chemistry of materials* **1996**, *8*, 1004.
(2) Luksic, S. A.; Riley, B. J.; Schweiger, M.; Hrma, P. *Journal of Nuclear Materials* **2015**, *466*, 526.
(3) Lukens, W. W.; Bucher, J. J.; Shuh, D. K.; Edelstein, N. M. *Environ. Sci. Technol.* **2005**, *39*, 8064.
(4) Fredrickson, J. K.; Zachara, J. M.; Plymale, A. E.; Heald, S. M.; McKinley, J. P.; Kennedy, D. W.; Liu, C.; Nachimuthu, P. *Geochimica et Cosmochimica Acta* **2009**, *73*, 2299.
(5) Navrotsky, A.; Mazeina, L.; Majzlan, J. *Science* **2008**, *319*, 1635.
(6) Buerge, I. J.; Hug, S. J. *Environmental Science & Technology* **1997**, *31*, 1426.
(7) Sedlak, D. L.; Chan, P. G. *Geochimica et Cosmochimica Acta* **1997**, *61*, 2185.
(8) Schlautman, M. A.; Han, I. *Water Research* **2001**, *35*, 1534.
(9) He, Y. T.; Chen; Traina, S. J. *Environmental Science & Technology* **2004**, *38*, 5535.

(10) Pettine, M.; D'Ottone, L.; Campanella, L.; Millero, F. J.; Passino, R. *Geochimica et Cosmochimica Acta* **1998**, *62*, 1509.
(11) He, Y. T.; Traina, S. J. *Environmental Science & Technology* **2005**, *39*, 4499.
(12) Kendelewicz, T.; Liu, P.; Doyle, C. S.; Brown Jr, G. E. *Surface Science* **2000**, *469*, 144.
(13) Kendelewicz, T.; Liu, P.; Doyle, C. S.; Brown Jr, G. E.; Nelson, E. J.; Chambers, S. A. *Surface Science* **1999**, *424*, 219.
(14) Pepper, S. E.; Bunker, D. J.; Bryan, N. D.; Livens, F. R.; Charnock, J. M.; Pattrick, R. A. D.; Collison, D. *Journal of Colloid and Interface Science* **2003**, *268*, 408.
(15) Marshall, T. A.; Morris, K.; Law, G. T. W.; Mosselmans, J. F. W.; Bots, P.; Parry, S. A.; Shaw, S. *Environmental Science & Technology* **2014**, *48*, 11853.
(16) Kobayashi, T.; Scheinost Andreas, C.; Fellhauer, D.; Gaona, X.; Altmaier, M. In *Radiochimica Acta International journal for chemical aspects of nuclear science and technology* 2013; Vol. 101, p 323.
(17) Peretyazhko, T. S.; Zachara, J. M.; Kukkadapu, R. K.; Heald, S. M.; Kutnyakov, I. V.; Resch, C. T.; Arey, B. W.; Wang, C. M.; Kovarik, L.; Phillips, J. L.; Moore, D. A. *Geochimica et Cosmochimica Acta* **2012**, *92*, 48.
(18) Smith, F. N.; Um, W.; Taylor, C. D.; Kim, D.-S.; Schweiger, M. J.; Kruger, A. A. *Environmental Science & Technology* **2016**, *50*, 5216.
(19) Skomurski, F. N.; Rosso, K. M.; Krupka, K. M.; McGrail, B. P. *Environmental Science & Technology* **2010**, *44*, 5855.
(20) Smith, F. N.; Taylor, C. D.; Um, W.; Kruger, A. A. *Environmental Science & Technology* **2015**, *49*, 13699.
(21) Um, W.; Chang, H.-S.; Icenhower, J. P.; Lukens, W. W.; Serne, R. J.; Qafoku, N. P.; Westsik, J. H.; Buck, E. C.; Smith, S. C. *Environmental Science & Technology* **2011**, *45*, 4904.
(22) Um, W.; Chang, H.; Icenhower, J. P.; Lukens, W. W.; Jeffrey Serne, R.; Qafoku, N.; Kukkadapu, R. K.; Westsik Jr, J. H. *Journal of Nuclear Materials* **2012**, *429*, 201.
(23) Lee, M.-S.; Um, W.; Wang, G.; Kruger, A. A.; Lukens, W. W.; Rousseau, R.; Glezakou, V.-A. *Nat Commun* **2016**, *7*.
(24) Muller, O.; White, W. B.; Roy, R. *Journal of Inorganic and Nuclear Chemistry* **1964**, *26*, 2075.
(25) McCarty, K. F.; Boehme, D. R. *Journal of Solid State Chemistry* **1989**, *79*, 19.
(26) Ma, M.; Zhang, Y.; Guo, Z.; Gu, N. *Nanoscale research letters* **2013**, *8*, 1.
(27) Schikorr, G. *Zeitschrift für Elektrochemie und angewandte physikalische Chemie* **1929**, *35*, 65.
(28) Russell, R. L.; Westsik Jr, J.; Swanberg, D. J.; Eibling, R. E.; Cozzi, A.; Lindberg, M. J.; Josephson, G. B.; Rinehart, D. E. *US Department of Energy Report PNNL* **2013**, *22352*.
(29) Webb, S. M. *Physica Scripta* **2005**, *2005*, 1011.
(30) Ravel, B.; Newville, M. *Journal of Synchrotron Radiation* **2005**, *12*, 537.
(31) Lukens, W. W.; Bucher, J. J.; Edelstein, N. M.; Shuh, D. K. *Environmental Science & Technology* **2002**, *36*, 1124.
(32) Wechsler, B. A.; Lindsley, D. H.; Prewitt, C. T. *American Mineralogist* **1984**, *69*, 754.
(33) Zachara, J. M.; Heald, S. M.; Jeon, B.-H.; Kukkadapu, R. K.; Liu, C.; McKinley, J. P.; Dohnalkova, A. C.; Moore, D. A. *Geochimica et Cosmochimica Acta* **2007**, *71*, 2137.
(34) Jolivet, J.-P.; Chanéac, C.; Tronc, E. *Chemical Communications* **2004**, 481.
(35) Pearce, C. I.; Qafoku, O.; Liu, J.; Arenholz, E.; Heald, S. M.; Kukkadapu, R. K.; Gorski, C. A.; Henderson, C. M. B.; Rosso, K. M. *Journal of colloid and interface science* **2012**, *387*, 24.

(36) Heald, S. M.; Krupka, K. M.; Brown, C. F. In *Radiochimica Acta International journal for chemical aspects of nuclear science and technology* 2012; Vol. 100, p 243.
(37) Heald, S. M.; Zachara, J. M.; Jeon, B.-H.; McKinley, J. P.; Kukkadapu, R.; Moore, D. *X-Ray Absorption Fine Structure--XAFS 13* **2007**, *882*, 173.
(38) Deer, W. A.; Howie, R. A.; Zussman, J. *An introduction to the rock-forming minerals*; 3 ed.; The Mineralogical Society: London, UK, 2013.
(39) Gorski, C. A.; Scherer, M. M. *American Mineralogist* **2010**, *95*, 1017.
(40) Shannon, R. *Acta Crystallographica Section A* **1976**, *32*, 751.
(41) Pearce, C. I. 2010.
(42) Sidhu, P. S.; Gilkes, R. J.; Posner, A. M. *Journal of Inorganic and Nuclear Chemistry* **1977**, *39*, 1953.

416 **Table 1.** Cr Oxidation State in Supernatant Determined by IC/ICP-MS

Sample[a]	Total Cr	Cr(VI)	Cr(III)
	ppm	*ppm*	*ppm*
	^{52}Cr		
Fe-DI-0.4-Cr-1	278	278	ND
Fe-DI-0.4-Cr-2	231	231	ND
	^{53}Cr		
Fe-DI-0.4-Cr-1	274	272	ND
Fe-DI-0.4-Cr-2	230	228	ND
	Average[b]		
Fe-DI-0.4-Cr-1	276(3)	275(4)	ND
Fe-DI-0.4-Cr-2	230(1)	230(2)	ND

ND: Non-detect, below the detection limit.

[a] Sample conditions: 1560 ppm Cr(VI), $Fe(OH)_2$:solution ratio = 0.01 g/mL, no Tc.

[b]Average values and standard deviation in parentheses determined from ^{52}Cr and ^{53}Cr data from each replicate sample.

417

418 **Table 2.** Solid Characterization Results for Cr-Containing Solids

$Fe(OH)_2$:Solution Ratio	Cr:Fe Ratio [a]	Cr Peak Fitting				Spinel a parameter [b]
		$FeCr_2O_4$	Cr_2O_3	$Cr(OH)_3$	Cr(VI)	
g/mL		*At%*	*At%*	*At%*	*At%*	*Å*
0.005	4.39	9.24	52.92	37.41	0.42	-
0.01	1.52	47.30	9.24	36.55	6.91	8.379(1)[c]
0.06	0.12	3.02	55.52	41.47	0	8.389(2)

[a] Cr:Fe ratio determined from the composition at% analysis for Fe, Cr, O, and C performed using the CasaXPS software.

[b]Spinel a parameter determined from XRD spectra using a magnetite reference to fit the spinel phase. Reference a parameters: magnetite = 8.396Å, chromite = 8.379Å, and maghemite = 8.34 Å.[38,39]

[c] Sample analyzed by XRD more than 30 days after sample preparation. Replicate sample, analyzed by XRD within 30 days of preparation, determined to have an a value = 8.3865(5) Å.

419

420